Efficient primary and parametric resonance excitation of bistable resonators

Cite as: AIP Advances **6**, 095307 (2016); https://doi.org/10.1063/1.4962843
Submitted: 26 July 2016 • Accepted: 02 September 2016 • Published Online: 12 September 2016

A. Ramini, N. Alcheikh, S. Ilyas, et al.

Efficient primary and parametric resonance excitation of bistable resonators

A. Ramini, N. Alcheikh, S. Ilyas, and M. I. Younis[a]
Physical Sciences and Engineering Division, King Abdullah University of Science and Technology, Thuwal 23955-9600, Saudi Arabia

(Received 26 July 2016; accepted 2 September 2016; published online 12 September 2016)

We experimentally demonstrate an efficient approach to excite primary and parametric (up to the 4th) resonance of Microelectromechanical system MEMS arch resonators with large vibrational amplitudes. A single crystal silicon in-plane arch microbeam is fabricated such that it can be excited axially from one of its ends by a parallel-plate electrode. Its micro/nano scale vibrations are transduced using a high speed camera. Through the parallel-plate electrode, a time varying electrostatic force is applied, which is converted into a time varying axial force that modulates dynamically the stiffness of the arch resonator. Due to the initial curvature of the structure, not only parametric excitation is induced, but also primary resonance. Experimental investigation is conducted comparing the response of the arch near primary resonance using the axial excitation to that of a classical parallel-plate actuation where the arch itself forms an electrode. The results show that the axial excitation can be more efficient and requires less power for primary resonance excitation. Moreover, unlike the classical method where the structure is vulnerable to the dynamic pull-in instability, the axial excitation technique can provide large amplitude motion while protecting the structure from pull-in. In addition to primary resonance, parametrical resonances are demonstrated at twice, one-half, and two-thirds the primary resonance frequency. The ability to actuate primary and/or parametric resonances can serve various applications, such as for resonator based logic and memory devices. [http://dx.doi.org/10.1063/1.4962843]

MEMS and Nano electromechanical systems (NEMS) resonators[1] have been proposed and used for various applications because of their small size, low fabrication and running cost, and their ultimate performance. These resonators have been employed in several applications, such as switches,[2,3] sensors,[4–7] RF amplifiers and filters,[8] and non-volatile memories.[9] Their operating principle is based on amplifying the output signal when the input frequency gets close to their resonance frequencies as a response to changes in their mass or stiffness by an external stimulus. Traditionally, resonators are designed to work in the linear regime and to avoid nonlinear behaviors. In contrast, their nonlinear behaviors have been proposed recently for various smart functionalities, such as for gas sensing.[10–12]

There are many sources of nonlinearity, such as electrostatic and magnetic actuation forces and the geometric nonlinearity in structures; particularly arched, buckled beams, and bistable structures.[13–19] Bistable structures are desired for various applications, such as energy harvesters, band pass filters, relays, switches, valves, actuators, and memory cells.

Parametric excitation in MEMS devices[20–22] is an attractive and intensively researched subject because of their ability to generate resonant responses in relatively wide bands of excitation frequencies as well as sharp transition between low-amplitude to large-amplitude responses upon changes in system parameters. Parametrically excited systems are appealing for many applications including sensing[23–25] and dynamic electromechanical amplifiers.[26–29] Many approaches were used

[a]Author to whom correspondence should be addressed. Electronic mail: Mohammad.younis@kaust.edu.sa.

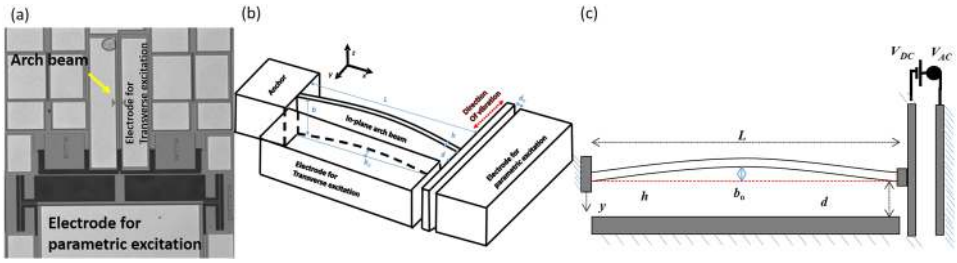

FIG. 1. (a) Optical microscopic image of the fabricated device. The arch beam is of 1000μm length, 25μm width, and 2μm thickness. The initial curvature of the arch b_o is 1.7μm. The gap between the arch beam and the transverse actuating electrode is 10.6μm. The gap between the side electrode and the stationary electrode of the parametric actuation is 5 μm. (b), (c) Schematics of the in-plane MEMS arch beam clamped at one end and connected at the other end by a link. The link is restricted to move in the x direction while the rotation is prevented. The straight red line represents the new deformed shape after applying the DC electrostatic force.

to achieve parametric excitation in MEMS and NEMS structures.[30–33] These mainly rely on modulating the mechanical stiffness of the structure by applying a time varying axial force, such as in strings[34] and beams.[35] Various ways have been reported to acquire time-dependent parametric force through electrostatic,[36] magnetic, piezoelectric, and thermal actuations.[37–39] Nano beams were also parametrically excited using modulated axial force through laser heating.[34–36]

The structure shown in Fig. 1(a) consists of an arch beam attached to an anchor at one end and connected at the other end to a stiff electrode, which is restricted to move in the x direction only with no rotation or transitional motion in the z and y directions, as shown in Fig. 1(b, c). The arch beam is flexible in the transverse direction (y direction). The movable stiff electrode forms one side of a parallel-plate capacitor oriented perpendicular to the arch beam (in the y direction) to generate the time varying axial electrostatic force. The electrostatic force consists of DC and AC components and acts in the x direction. These results in a time varying axial force applied to the beam, which leads to the parametric excitation. The geometrical parameters of the two case studies of arches under consideration are listed in Table I.

The arches are fabricated using single crystal silicon of thickness 25 μm by a two-mask fabrication process.[40] It is worth mentioning that while the electrostatic force is inherently nonlinear, this nonlinearity can be neglected for the parametric excitation since the axial displacement of the beam side, and hence the displacement of the side electrode, is very small.

We used an in-plane stroboscopic video microscopy for the motion analysis in the in-plane direction. In order to measure the linear resonance frequencies of the devices, we subjected them to ring-down test (sudden application of unit step voltage load) and extracted the fast Fourier transforms FFTs of the response. The measurements, Fig. 2(a, b), show the first primary resonance frequency, for case A at *40.5 kHz* and for case B at *14.72 kHz*.

In the case of exciting the structures in the neighborhoods of the fundamental resonance frequency under vacuum conditions, which is also considered the second parametric resonance regime, different frequency response curves corresponding to different voltage amplitudes are shown for both cases in Fig. 2 (c, d). One observes that the resonator of case A shows a softening behavior around the

TABLE I. The measured dimensions of the tested structures.

	Case A	Case B
Length (L)	600 μm	1000 μm
Width (b)	25 μm	25 μm
Thickness (h)	2 μm	2 μm
Gap (d)	7.6 μm	10.6 μm
Initial curvature (b_o)	2.7 μm	1.7 μm
The gap for the parametric actuation	2 μm	5 μm

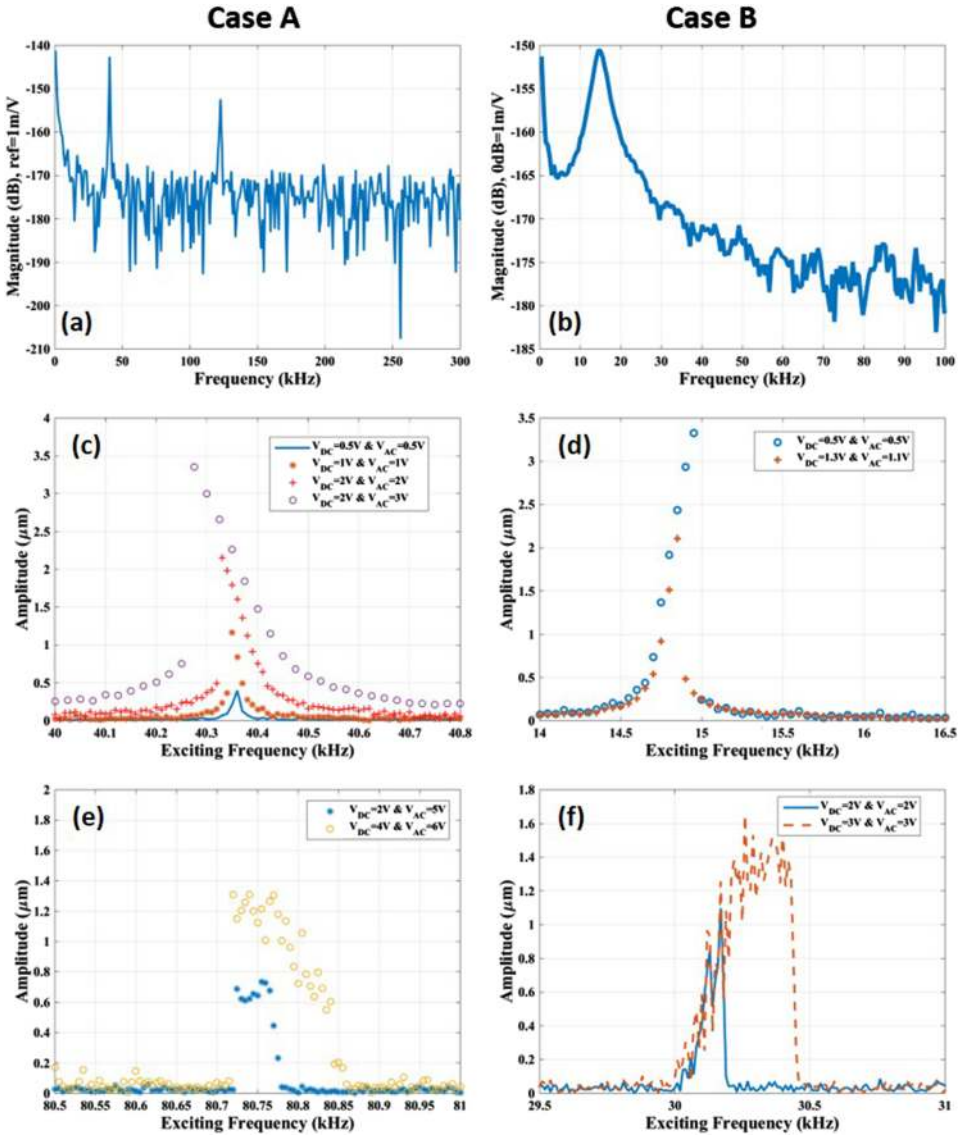

FIG. 2. Frequency responses of the two case studies. (a), (b): FFTs of the response revealing the resonance frequencies for (a) case A and (b) case B. (c), (d): Experimental frequency response curves corresponding to different voltage amplitudes using the parametric axial forcing in the vicinity of the primary resonance for case A (c) and case B (d). (e), (f): Experimental frequency responses corresponding to different voltage amplitudes in the vicinity of first principal parametric resonance for case A (e) and case B (f).

primary resonance; on the other hand, case B exhibits hardening behavior. This is because the initial curvature in case B is small; and hence, the arch behaves more like a straight beam with a dominant cubic nonlinearity causing hardening effect. On the other hand, the arch of case A has larger initial rise making the quadratic nonlinearity from the curvature dominant; and thus it exhibits softening behavior.[41]

One notes from Fig. 2 (c, d) that despite the parametric excitation, the arches do not show characteristics of parametric resonances (no sudden jumps between the lower and upper branches as in pitchfork bifurcations); rather they show features of a classical primary resonance. Due the initial curvature of the arch, an axial force has components that excite a vertical motion of the arch, as in external force excitation, in addition to the parametric (pure axial) component. Thus, we believe that the behavior is a mixed response between primary and 2^{nd} parametric responses in the vicinity of the fundamental resonance frequency; however, with the primary resonance has more dominant effect.

It is practically difficult to differentiate between the contributions of the primary and 2^{nd} parametric resonance responses on the total resonator response.

In the vicinity of the first principal parametric resonance (near twice the fundamental natural frequency), the frequency response curves for different voltage loads are shown in Fig. 2(e, f). The curves show parametric resonance for both cases where their amplitudes increase with the increase in voltage loads.

Next, we compare for case B the response near the fundamental natural frequency (primary resonance) when exciting the structure using a classical transverse electrostatic actuation, where the arch serves as an electrode itself, to the case when excited axially and electrostatically from the side, Fig. 3. One notes that less actuation voltage is required in the classical electrostatic actuation to obtain the same response level due to the axial "parametric" actuation under atmospheric pressure conditions, Fig. 3(a, b). However, the parametric actuation generates higher amplitude vibrations compared to the transverse electrostatic forcing under vacuum conditions, Fig. 3(c, d). Figure 3 implies that the squeeze film damping in the axial (side) parallel-plate actuation reduces the effect of the time varying axial force. Note that such effect is much less in the transverse case due to the large capacitive gap in this case. Decreasing the pressure reduces the effect of the squeeze film damping. Consequently, in near vacuum conditions, the vibrational amplitude has higher amplitude in the case of the axial force excitation compared to the external parallel plate actuation.

In the case of actuation in the vicinity of the third parametric resonances ($f_{excitation} = f_{3rd\ parametric} = 2/3\ f_n$), Fig. 4(a) shows a frequency response curve of this case for $V_{DC} = 10V$ and $V_{AC} = 38V$. We also experimentally show the displacement of the steady state response of the last period at the maximum amplitude, Fig. 4(b), as well as the phase portrait, Fig. 4(c), that shows 3 looping circles.

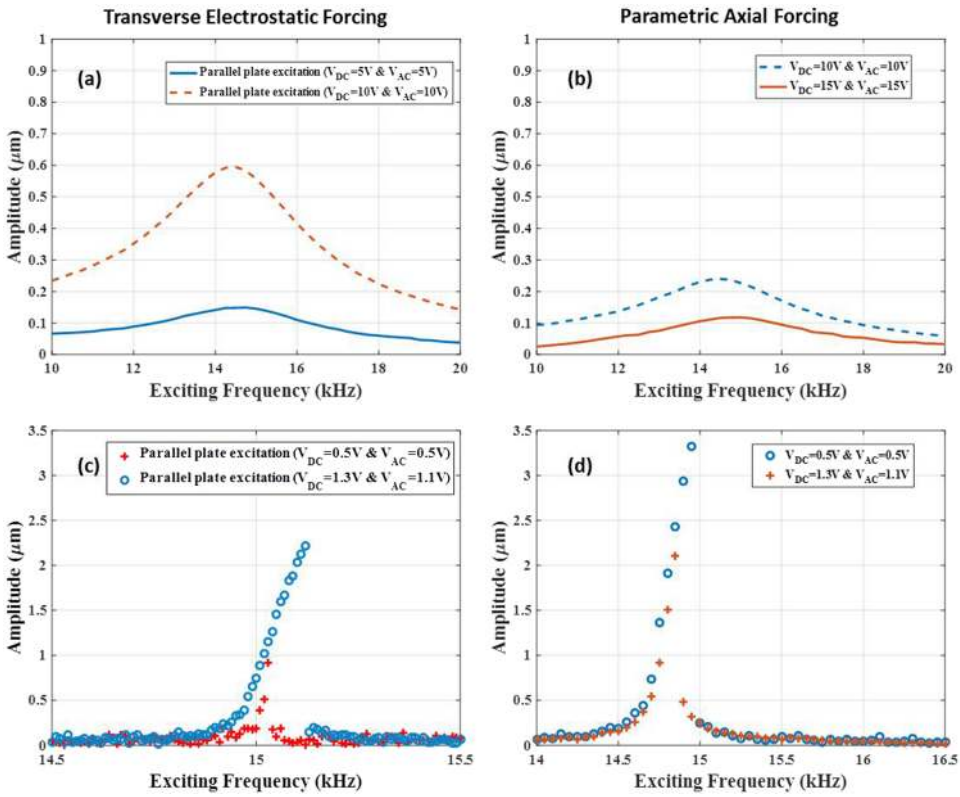

FIG. 3. Experimental frequency response curves due to two excitation methods for case B: (a) Using the electrode of the transverse actuation (external electrostatic actuation) under atmospheric pressure. (b) Using the parametric axial forcing under atmospheric pressure. (c) Using external electrostatic actuation under vacuum conditions. (d) Using the parametric axial forcing under vacuum conditions.

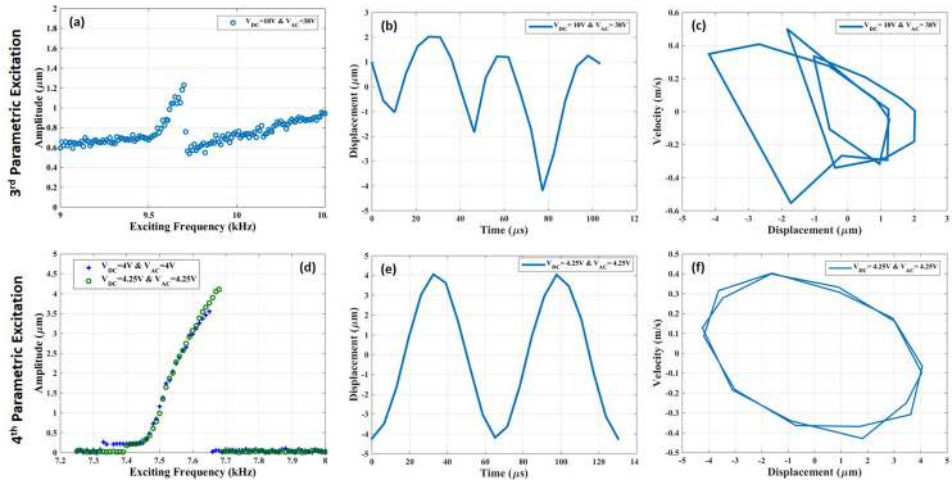

FIG. 4. Experimental tests for case B. (a) A frequency response at $V_{DC} = 10V$ and $V_{AC} = 38V$ for the 3^{rd} parametric excitation, (b) the maximum steady displacement at $9.7\ kHz$ and (c) the experimental phase portrait at $9.7\ kHz$ for 3^{rd} parametric excitation. For the 4^{th} parametric excitation, (d) an experimental frequency response corresponding to different voltage amplitudes, (e) the maximum steady displacement at $7.68\ kHz$, and (f) the experimental phase portrait at $7.68\ kHz$.

This dynamic response at ($f_{3rd\ parametric} = 2/3\ f_n$) is a strong indication of the parametric excitation, even if a mixed response around the primary resonance (2^{nd} parametric) exists.

Figure 4(d) shows the actuation in the vicinity of the fourth parametric resonance ($f_{excitation} = f_{4th\ parametric} = 1/2\ f_n$) for different voltage loads. Here again the dynamic response can be viewed as a mixed response between the parametric and superharmonic response (of order half due to the quadratic nonlinearity). Like the response around the fundamental resonance frequency, it is difficult to differentiate between the two responses. Here, the dynamic response has larger amplitude of vibration, Fig. 4(e), compared to the vibrational amplitude of the 1^{st} and 3^{rd} parametric resonances with less voltage loads. As a result, the phase portrait around ($1/2\ f_n$.) demonstrates the dominance of the superharmonic behavior that shows as two circles in Fig. 4(f). Using a camera frame measurement technique, it is difficult to obtain clear results near the 3rd and 4th parametric resonances because of the emergence of the primary resonance frequency in the response in addition to the excitation frequency, which interferes with the camera system that is synchronized to a single frequency (the excitation one).

One of the advantages of the proposed excitation approach is the ability to shift and tune the operating resonance frequencies by the DC voltage, as shown in Fig. 5, and consequentially shifting and tuning the parametric ones. Figure 5 indicates that increasing the DC voltage increases the axial

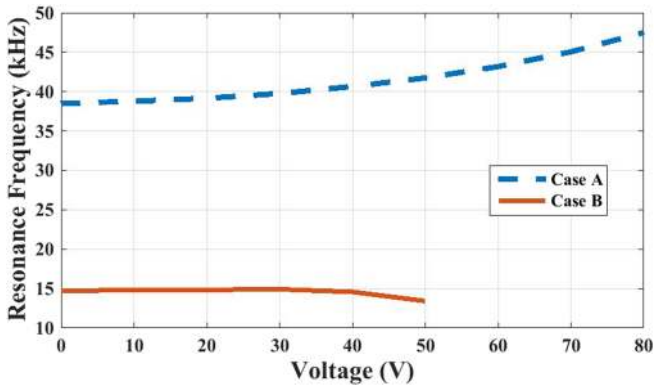

FIG. 5. Frequency shift of the primary resonance frequency by applying static axial tensile force generated through the voltage applied on the side electrode. Case A has $f_n = 40.5\ kHz$ at zero voltage. Case B has $f_n = 14.72\ kHz$ at zero voltage.

tension in the structures and shifts the fundamental resonance frequency causing stiffening of the structure in case A and softening of the structure in case B. This can be valuable for inertial sensors and mechanical resonators for mass detection and logic gates.

Another distinctive feature of the actuation approach here is the combination of large vibrational amplitudes of the arch beam and low electrostatic actuation compared to the typical parallel-plate electrode actuation, shown in Fig. 3. In parallel-plate transductors, the small electrostatic gap limits achieving considerable deflections of the actuated structures, hence decreasing their efficiency. Also, these devices usually suffer from static and dynamic pull-in instabilities preventing the ability to achieve large displacements. In addition, using the axial force prevents other undesirable instabilities in arch beam, such as snap-through and chaotic behaviors. The approach presented here allows overcoming these crucial difficulties because the direction of the actuation force is perpendicular to the direction of the vibrations.[42] Moreover, the nonlinearity introduced by the electrostatic force plays negligible role on the parametric excitation and imposes no restrictions on the actuating force. This arch beam with parametric actuation can be considered, in a sense, as a dynamic parametric motion transformer and amplifier because the lateral vibrational amplitudes are significantly larger than the axial deflection. The reported dynamics of these MEMS arches structures are important and relevant to a wide range of applications starting from micro-scale devices going down in size to nano-scale structure and NEMS sensors.

To summarize, we reported on the experimental results of parametrically excited MEMS arch resonators by a time varying axial force that is generated through an electrostatically actuated movable electrode at one of the ends. This axial force results in the variation of its curvature and mechanical stiffness and accordingly actuates the resonators primarily and parametrically. Parametric resonant responses were observed and shown at twice, half, and two-thirds the first fundamental resonance frequency, in addition to the primary resonance of the fundamental mode. Our approach overcomes crucial difficulties limiting large amplitude vibrations, such as static and dynamic pull-in instabilities. Finally, this parametric dynamic approach may have applications extending to multi-stable, MEMS and NEMS logic[43] and memory.

See supplementary material for Arch Resonator Amplitude and Frequency: The motion of the resonator was detected optically using a stroboscopic video microscopy for in-plane motion analysis. After reaching steady state vibration, the amplitude of the last period was calculated at each frequency step of the frequency sweep. These videos: video 1 shows 1st parametric response at 80.72 kHz for case A, videos 2 and 3 show 3rd parametric response at 9.7 kHz and 4th parametric response at 7.68 kHz for case B

[1] H. C. Nathanson, W. E. Newell, R. A. Wickstrom, and J. R. Davis, IEEE Trans. Electron. Dev. **14**, 117–33 (1967).
[2] V. Intaraprasonk and S. Fan, Appl. Phys. Lett. **98**, 241104 (2011).
[3] F. K. Chowdhury, D. Saab, and M. Tabib-Azar, Sens. Actuators, A **188**, 481 (2012).
[4] X. M. H. Huang, M. Manolidis, S. C. Jun, and J. Hone, Appl. Phys. Lett. **86**, 143104 (2005).
[5] B. Ilic, Y. Yang, K. Aubin, R. Reichenbach, S. Krylov, and H. G. Craighead, Nano Lett. **5**, 925–9 (2005).
[6] D. R. Southworth, L. M. Bellan, Y. Linzon, H. G. Craighead, and J. M. Parpia, Appl. Phys. Lett. **96**, 163503 (2010).
[7] R. Harne and K. Wang, J. Sound Vib. **333**, 2241 (2014).
[8] G. M. Rebeiz, *RF MEMS: Theory Design and Technology* (Wiley Interscience, Hoboken, NJ, 2003).
[9] B. Charlot, W. Sun, K. Yamashita, H. Fujita, and H. Toshiyoshi, J. Micromech. Microeng. **18**, 045005 (2008).
[10] B. DeMartini, J. Rhoads, M. Zielke, K. Owen, S. Shaw, and K. Turner, Appl. Phys. Lett. **93**, 054102 (2008).
[11] V. Kumar, J. Boley, Y. Yang, H. Ekowaluyo, J. Miller, G. Chiu, and J. Rhoads, Appl. Phys. Lett. **98**, 153510 (2011).
[12] A. Bouchaala, N. Jaber, O. Shekhah, V. Chernikova, M. Eddaoudi, and M. Younis, Appl. Phys. Lett. **109**(1), 013502 (2016).
[13] M. I. Younis, *MEMS Linear and Nonlinear Statics and Dynamics* (Springer, 2011).
[14] R. Harne, M. Thota, and K. Wang, Appl. Phys. Lett. **102**, 053903 (2013).
[15] A. F. Arrieta, P. Hagedorn, A. Erturk, and D. J. Inman, Appl. Phys. Lett. **97**, 104102 (2010).
[16] C. Lan, W. Qin, and W. Deng, Appl. Phys. Lett. **107**, 093902 (2015).
[17] L. Medina, R. Gilat, B. R. Ilic, and S. Krylov, Appl. Phys. Lett. **108**, 073503 (2016).
[18] A. Ramini, M. L. F. Bellaredj, M. Al-Hafiz, and M. I. Younis, J. Micromech. and Microeng. **26**(1), 015012 (2015).
[19] A. Ramini, Q. M. Hennawi, and M. I. Younis, J. Microelectromech. Syst. **25**(3), 570–578 (2016).
[20] K. L. Turner, S. A. Miller, P. G. Hartwell, N. C. MacDonald, S. H. Strogatz, and S. G. Adams, Nature **396**(6707), 149–152 (1998).
[21] S. Krylov, I. Harari, and Y. Cohen, J. Micromech. Microeng. **15**, 1188–204 (2005).
[22] I. Mahboob and H. Yamaguchi, Nature Nanotechnology **3**, 275–279 (2008).
[23] W. Zhang and K. L. Turner, Sensors Actuators A **122**, 23–30 (2005).
[24] M. V. Requa and K. L. Turner, Appl. Phys. Lett. **88**, 263508 (2006).

[25] D. Rugar and P. Grütter, Phys. Rev. Lett. **67**, 699–702 (1991).
[26] D. W. Carr, S. Evoy, L. Sekaric, H. G. Craighead, and J. M. Parpia, Appl. Phys. Lett. **77**, 1545–7 (2000).
[27] I. Mahboob and H. Yamaguchi, Appl. Phys. Lett. **92**, 173109 (2008).
[28] I. Mahboob and H. Yamaguchi, Appl. Phys. Lett. **92**, 253109 (2008).
[29] J. F. Rhoads and S. W. Shaw, Appl. Phys. Lett. **96**, 234101 (2010).
[30] M. Napoli, R. Baskaran, K. L. Turner, and B. Bamieh, Proc. IEEE 16th Int. Ann. Conf. MEMS (MEMS' 2003), 169–72 (2003).
[31] W. Zhan, R. Baskaran, and K. Turner, Appl. Phys. Lett. **82**, 130 (2003).
[32] Y. C. Hu, C. M. Chang, and S. C. Huang, Sensors Actuators A **112**, 155–61 (2004).
[33] S. K. De and N. R. Aluru, Phys. Rev. Lett. **94**, 204101 (2005).
[34] R. D. Rowland, Am. J. Phys. **72**, 758–66 (2004).
[35] A. H. Nayfeh and D. T. Mook, *Nonlinear Oscillations* (Wiley, NewYork: Wiley, 1979).
[36] S. Krylov, Y. Gerson, T. Nachmias, and U. Keren, J. Micromech. Microeng. **20**, 015041 (2010).
[37] K. Aubin, M. Zalalutdinov, A. Tuncay, R. B. Reichenbach, R. H. Rand, A. T. Zehnder, J. Parpia, and H. G. Craighead, J. Microelectromech. Syst. **13**, 1018–26 (2004).
[38] M. Pandey, K. Aubin, M. Zalalutdinov, R. B. Reichenbach, A. T. Zehnder, R. H. Rand, and H. G. Craighead, J. Microelectromech. Syst. **15**, 1564–54 (2006).
[39] M. Zalalutdinov, A. Olkhovets, A. Zehnder, B. Ilic, D. Czaplewski, H. G. Craighead, and J. M. Parpia, Appl. Phys. Lett. **78**, 3142–4 (2001).
[40] MEMSCAP, http://www.memscap.com.
[41] H. M. Ouakad and M. I. Younis, Int. J. of Non-Linear Mech. **45**(7), 704–713 (2010).
[42] N. Kacem, S. Baguet, L. Duraffourg, G. Jourdan, R. Dufour, and S. Hentz, Appl. Phys. Lett. **107**, 073105 (2015).
[43] M. A. A. Hafiz, L. Kosuru, and M. I. Younis, Nature Commun. **7**, 11137 (2016).